Supplement of Atmos. Chem. Phys., 15, 10093–10106, 2015
http://www.atmos-chem-phys.net/15/10093/2015/
doi:10.5194/acp-15-10093-2015-supplement

Supplement of

Impact of climate and land cover changes on tropospheric ozone air quality and public health in East Asia between 1980 and 2010

Y. Fu and A. P. K. Tai

Correspondence to: A. P. K. Tai (amostai@cuhk.edu.hk)

Supplementary Materials

S1. Detail land cover and land use data

The Moderate Resolution Imaging Spectroradiometer (MODIS) satellite-derived high-resolution land cover product for year 2010 is used as the baseline case in this work (MCD12Q1) (https://lpdaac.usgs.gov/products/modis_products_table/mcd12q1). This product includes five land cover classification schemes. Here we choose the classification scheme of IGBP (International Geosphere-Biosphere Program) with 17 land cover types, including 13 vegetation classes (evergreen needleleaf forest, evergreen broadleaf forest, deciduous needleleaf forest, deciduous broadleaf forest, mixed forest, closed shrublands, open shrublands, woody savannas, savannas, grasslands, permanent wetlands, croplands, cropland/natural vegetation mosaic) and 4 non-vegetated land types (water, urban and built-up, snow and ice, barren or sparsely vegetated). We further combine them with the Koppen main climate classes following Steinkamp and Lawrence (2011). As a result, a new land cover map MODIS-IGBP-Koppen in year 2010 with 23 land cover types is developed. The distribution of land cover and land use types in year 2010 used in this study are shown in Fig. S1.

To derived the land cover and land use in year 1980, we produce the potential land cover map by integrating multiple sources of data and information, including the MODIS-IGBP land cover data in 2005, the Koppen main climate classes map, the China National land cover dataset (NLCD) for the late 1980s and year 2005 (Liu and Buheaosier, 2000; Liu et al., 2005a, b), and the harmonized historical cropland and urban land use dataset from the historical land cover projects of Representative Concentrationthe Pathways (RCPs) for the period 1980-2005 from Hurtt et al.(2011). To ensure the self-consistency of the PFT across the period, we assume that the PFT definition and the vegetation composition for each PFT remained unchanged. The MODIS-IGBP-Koppen land map in 2005 is developed through combining the MODIS-IGBP land cover data in 2005 with the Koppen main classes following the same methods of generating the MODIS-IGBP-Koppen land cover types in 2010. The reconstructed cropland and urban areas are based on the HYDE model which combines numerous historical statistics, census data and satellite-derived current land cover from DISCover 2 data (Loveland et al., 2000) and Global Land Cover (GLC 2000) (Bartholome et al., 2002). The method we use to reconstruct the land cover and land use in 1980 is similar to that of Liu and Tian (2010), and is based on the MODIS-IGBP-Koppen LCLU in year 2005 as base year and applies appropriate calibration ratios to scale up/down the 2005 data. For instance, cropland and urban fractional coverage in year 1980 in each model grid cell is obtained by scaling up/down the MODIS-IGBP-Koppen value in 2005 with a calibration ratio derived from the slope of time-series linear regression of 1980-2005 harmonized RCP data. For each of the other natural vegetation types, the calibration ratio is an overall ratio derived from the slope of reduced major-axis regression between NLCD 1980s and NLCD 2005 available data over the whole spatial domain. It should be noted that the sum of fractional coverages of all PFTs including bareland of each grid cell is always constrained to unity.

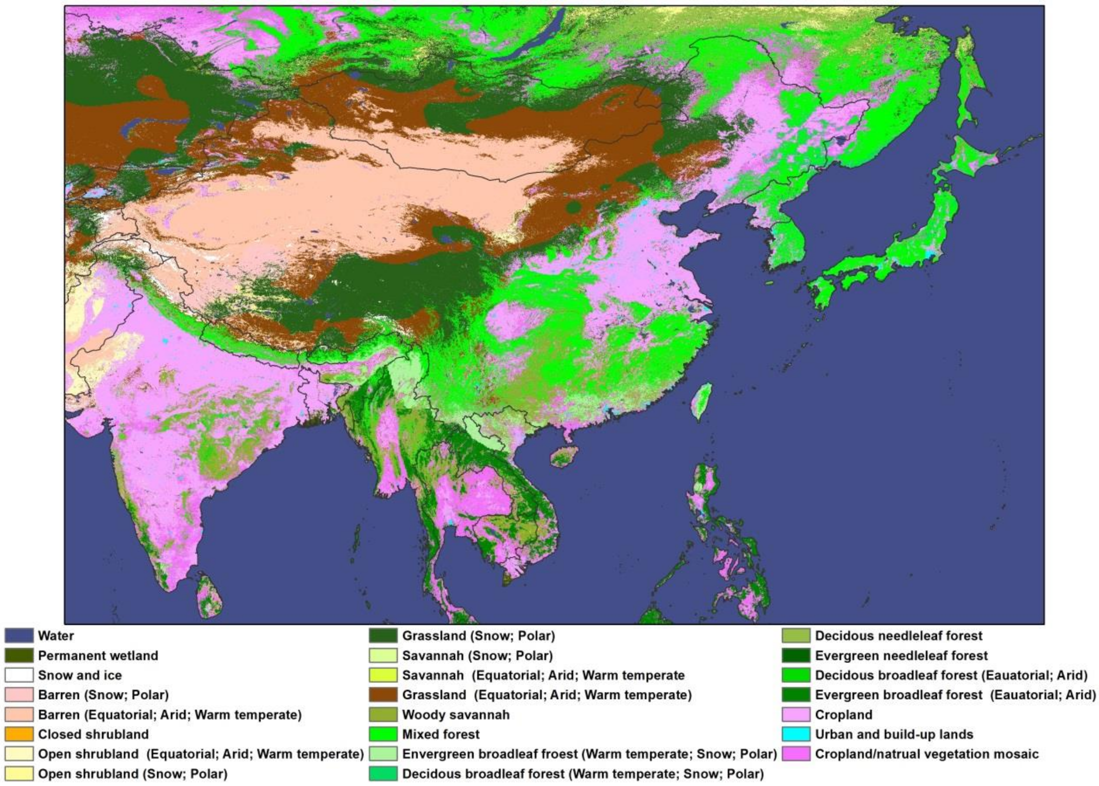

Fig. S1. Land cover and land use distribution in year 2010.

S2. Changes in biogenic VOC emissions

Annual isoprene emission in East Asia decreases by 3% but increases by 2% in China specifically as a result of LCLU change alone between 1980 and 2010 ([*CTRL*]-[*SIM_LCLU*]) (Table S4). Our calculated decreases (increases) in isoprene emission in East Asia (China) generally agree with Stavrakou et al. (2014). Seasonal and regional isoprene emission exhibits more pronounced changes in response to LCLU change. In summer (JJA), we find that the seasonal mean isoprene emission increases 5-30% in central and southeastern China but decreases 5-20% over northeastern China, Korea and Myanmar (Fig.2b). Changes in JJA isoprene emission are consistent in spatial distribution with the changes in forest coverage (Fig. S2a). Increases in JJA isoprene emission are likely caused by the enhanced fractional coverage of broadleaf and mixed forests, while the reduction of isoprene emission results from the reduced coverage of both needleleaf and broadleaf forests over those regions. In spring (MAM), LCLU change alone reduces isoprene emission by as much as 40% in eastern China, Korea, and Southeast Asia (Fig. 3b). Such a decrease is primarily driven by reduced LAI in most of East Asia (Fig. 1b).

Climate change alone increases annual isoprene emission in East Asia by 7.4% ([*CTRL*]-[*SIM_CLIM*]) (Table S4). In summer, isoprene emission increases by 5-20% in most places of East Asia (Fig. S2b). In spring, isoprene emission increases by 5-40% in southern China and parts of Southeast Asia, while isoprene emission in Myanmar, northern China and Japan decreases by 5-30% due to climate change alone.

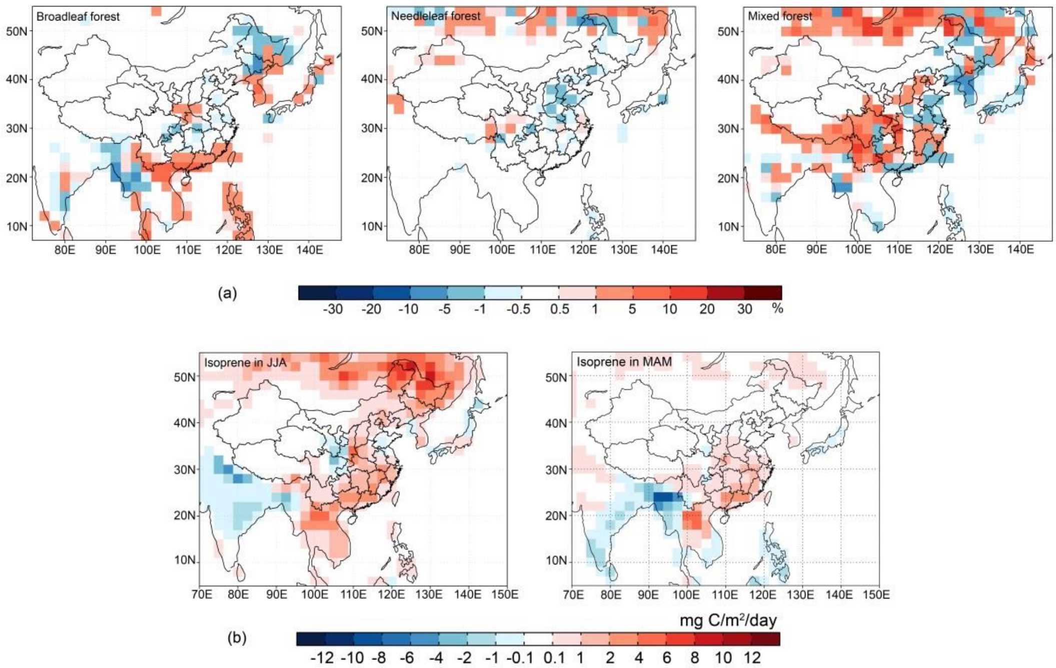

Fig. S2. Changes in (a) fractional coverage of broadleaf, needleleaf, and mixed forests; and (b) in isoprene emission in summer (JJA) and spring (MAM) driven by climate change alone from the period 1981-1985 to the period 2007-2011.

S3. Effects of changes in vegetation distribution alone and in density alone between 1980 and 2010

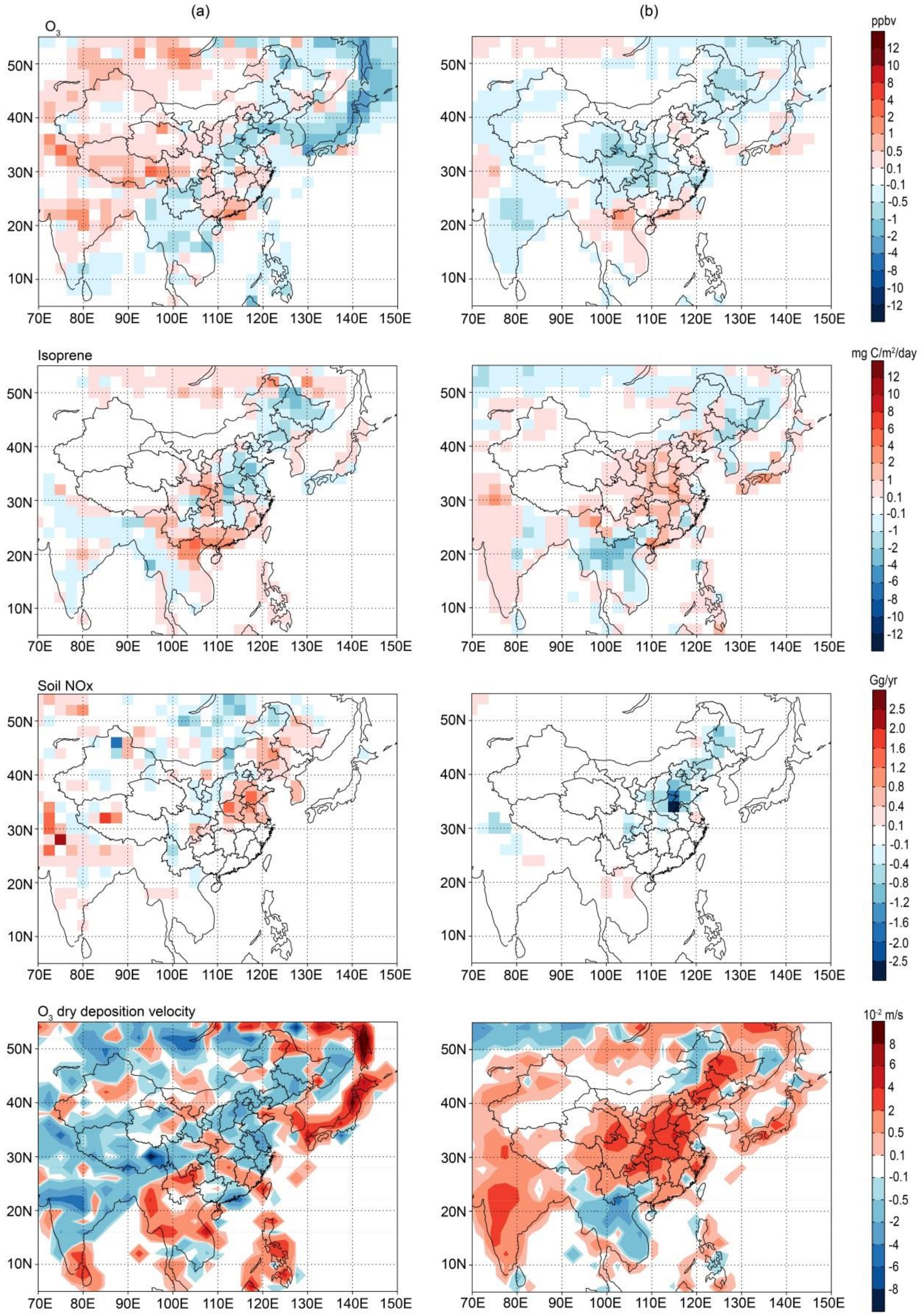

Fig. S3. Changes in summertime surface ozone, isoprene emission, soil NO_x emission, and dry deposition velocity arising from changes in (a) vegetation distribution (represented by PFT fractional coverage) alone ([*CTRL_2010*]-[*SIM_PFT*]) and (b) vegetation density (represented by LAI) alone ([*CTRL_2010*]-[*SIM_LAI*]).

S4. Effects of changes in temperature alone and relative humidity alone

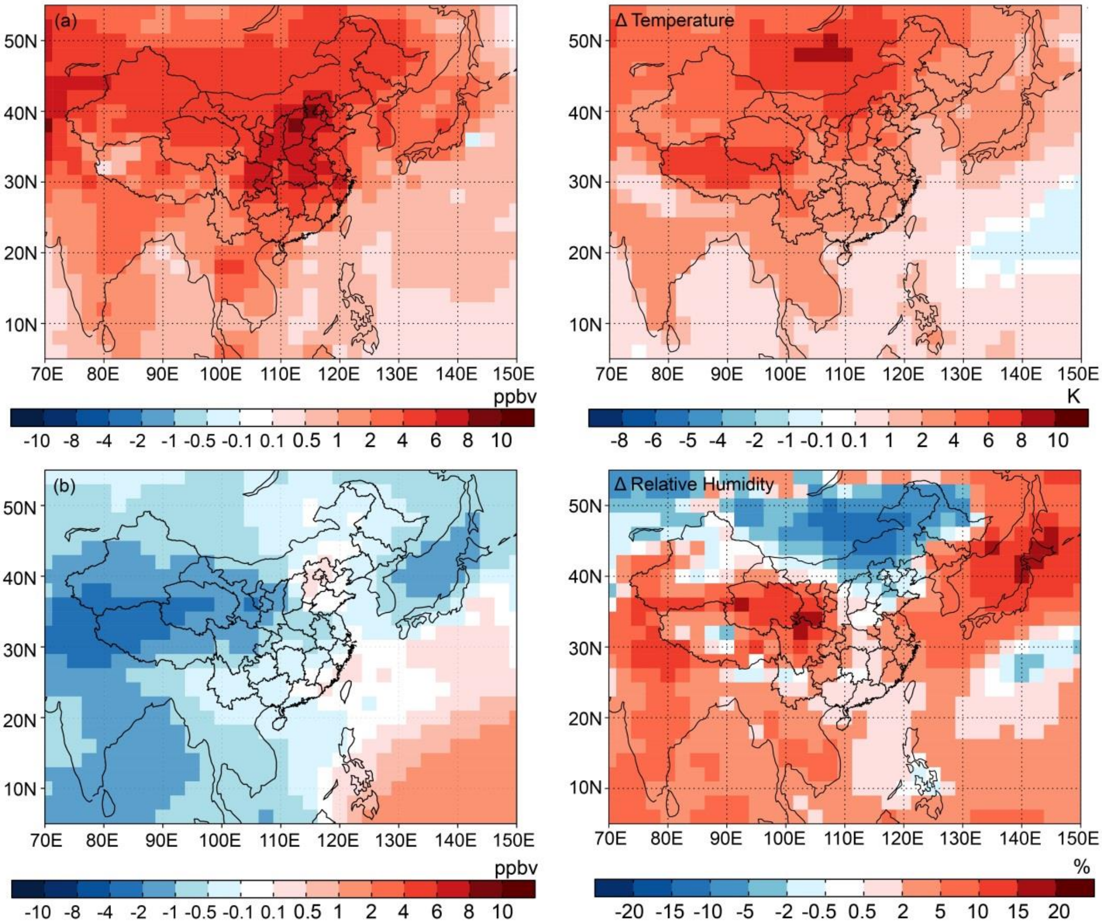

Fig. S4. Changes in surface maximum daily 8-hour average ozone concentration (MDA8 O_3) driven by changes in (a) temperature alone ([*CTRL_2010*]-[*SIM_TMP*]); and (b) relative humidity alone ([*CTRL_2010*]-[*SIM_RH*]).

S5. Interannual variations of ozone concentration in simulation CTRL and COMB

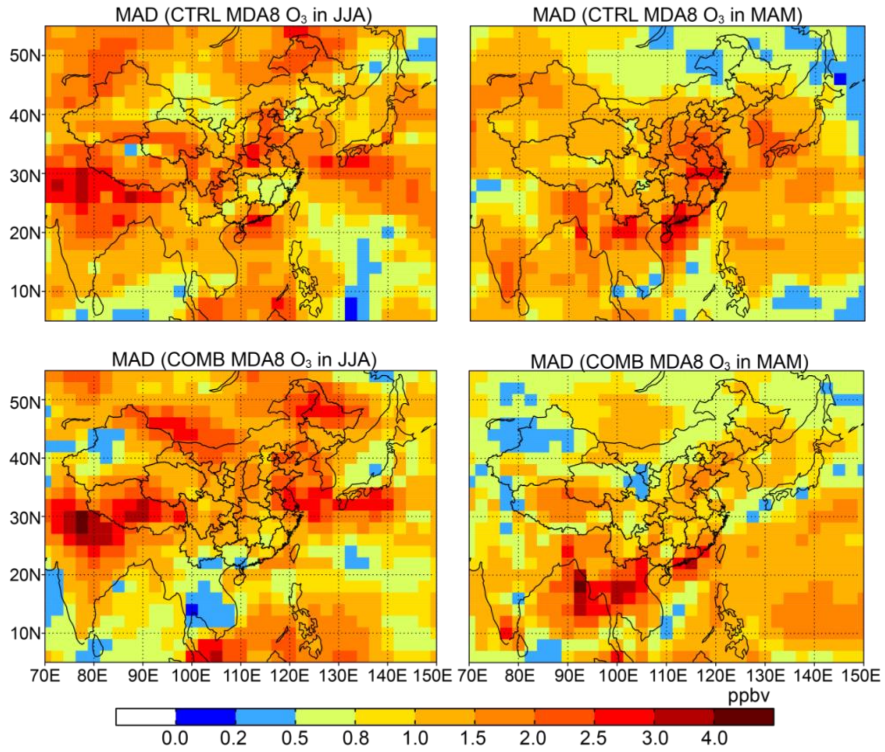

Fig. S5. Mean absolute deviation (MAD) of surface ozone in JJA and MAM from the simulations CTRL (2007-2011) and the simulations COMB (1981-1985).

S6. Method for assessing the health impact due to ozone air quality

Since there are very limited studies reporting long-term ozone-related mortality in East Asia, we apply epidemiological concentration-response functions (CRFs) from American Cancer Society (ACS) in this study. As in Anenberg et al (2010) and Silva et al (2013), we use surface ozone concentrations to estimate excess ozone-related respiratory mortality (ΔM, unit: 1000 deaths per year per squared km) by applying the following CRFs (Anenberg et al., 2010):

$$\Delta M = y_0\left(1 - e^{-\beta \Delta X}\right)P$$

where y_0 represents the baseline mortality rate (unit: deaths per thousand people per year), β is a concentration-response factor, ΔX represents the differences in ozone concentrations (April-September 6-month averaged of 1-h daily maximum ozone concentration (Jerrett et al., 2009)), and P is the exposed population (unit: people per squared km). Consistent with ACS, we only assess ozone-related health impact for all adults aged 30 and above. We use gridded population of the world at approximately 0.5°×0.5° resolution from Socioeconomic Data and Applications Center (SEDAC), Columbia University (version 3 for future estimates in year 2010; http://sedac.ciesin.columbia.edu/data/set/gpw-v3-population-density-future-estimates, accessed by 7 November 2014) and United Nations estimates of 2010 population by age-group per country (World Population Prospects, 2012 revision, http://esa.un.org/unpd/wpp/Excel-Data/population.htm, accessed by 7 November 2014) to calculate the fraction of population aged 30 and above at the country level and the exposed population aged 30 and above in East Asia. Then, the exposed population over 30 is regridded to 2°×2.5° resolution consistent with that of the simulated ozone concentrations.

Baseline mortality rates for respiratory disease are calculated from the World Health Organization 2000-2012 country-level cause-specific mortality for population aged 30 or above (http://www.who.int/healthinfo/global_burden_disease/estimates/en/index1.html, accessed by 7 November 2014). The concentration-response factor is derived from relative risks (RR) estimated in long-term epidemiological studies, which is represented as a log-linear relationship between ozone concentration and RR (β = ln(RR)/10) (Jerrett et al., 2009).

Table S1. PFT-specific emission factors* for biogenic VOC emissions used in this study (units: μg m^{-2} h^{-1}).

Compound Class / PFTs	Isoprene	Monoterpenes							MBO	Acetone
		α-Pinene	β-Pinene	Myrcene	Sabinene	Limonene	3-Carene	Ocimene		
Evergreen broadleaf forest *(warm temperate; snow; polar)*	10000	400	130	30	50	80	30	120	0.01	240
Decidous broadleaf forest *(warm temperate; snow; polar)*	10000	400	130	30	50	80	30	120	0.01	240
Decidous needleleaf forest	1	510	200	60	40	130	80	60	0.01	240
Evergreen needleleaf forest	3000	500	300	70	70	100	160	70	60	240
Decidous broadleaf forest *(equatorial; arid)*	7000	600	120	80	80	80	40	150	0.01	240
Evergreen broadleaf forest *(equatorial; arid)*	7000	600	120	80	80	80	40	150	0.01	240
Closed shrubland	4000	200	100	30	50	60	30	90	0.01	240
Open shrubland *(equatorial; arid; warm temperate)*	2000	200	100	30	50	60	30	90	0.01	240
Open shrubland *(snow; polar)*	2000	200	100	30	50	60	30	90	0.01	240
Grassland *(snow; polar)*	1600	2	1.5	0.3	0.7	0.7	0.3	2	0.01	80
Savannah *(snow; polar)*	1600	2	1.5	0.3	0.7	0.7	0.3	2	0.01	80
Savannah *(equatorial; arid; warm temperate)*	800	2	1.5	0.3	0.7	0.7	0.3	2	0.01	80
Grassland *(equatorial; arid; warm temperate)*	800	2	1.5	0.3	0.7	0.7	0.3	2	0.01	80
Woody savannah	4000	300	150	50	70	100	100	150	0.01	240
Cropland	1	2	1.5	0.3	0.7	0.7	0.3	2	0.01	80
Mixed forest	Assumed the coverage are equally divided into 4 types of broadleaf trees and 2 types of needleleaf trees									
Cropland/natural vegetation mosaic	Assumed the coverage are divided into cropland (40%), shrubland (30%) and grassland (30%)									

* Guenther et al. (2012)

Table S2. Method for merging 23 land types into 5 MEGAN PFTs.

No.	MODIS_Koppen land type	MEGAN PFT
1	Water	-
2	Permanent wetland	-
3	Snow and ice	-
4	Barren (snow; polar)	-
5	Unclassified	-
6	Barren (equatorial; arid; warm temperate)	-
7	Closed shrubland	Shrub
8	Open shrubland (equatorial; arid; warm temperate)	Shrub
9	Open shrubland (snow; polar)	Shrub
10	Grassland (snow; polar)	Grass
11	Savannah (snow; polar)	Grass
12	Savannah (equatorial; arid; warm temperate)	Grass
13	Grassland (equatorial; arid; warm temperate)	Grass
14	Woody savannah	Shrub
15	Mixed forest	Assume Mixed forest consist of 30% broadleaf trees and 70% needleleaf trees
16	Evergreen broadleaf forest (warm temperate; snow; polar)	Broadleaf trees
17	Deciduous broadleaf forest (warm temperate; snow; polar)	Broadleaf trees
18	Deciduous needleleaf forest	Needleleaf trees
19	Evergreen needleleaf forest	Needleleaf trees
20	Deciduous broadleaf forest (equatorial; arid)	Broadleaf trees
21	Evergreen broadleaf forest (equatorial; arid)	Broadleaf trees
22	Cropland	Crop
23	Urban and built-up lands	-
24	Cropland/natural vegetation mosaic	Assume this type composes of 40% crop, 30% shrub and 30% grass.

Table S3. Mapping 23 land types into Olson land types used for dry deposition.

NO	MODIS_Koppen land types	Olson ID	Olson land types*
1	Water	0	water
2	Permanent wetland	45	wetland
3	Snow and ice	17	Ice
4	Barren (snow; polar)	53	Barren tundra
5	unclassified	-	Not used
6	Barren (equatorial; arid; warm temperate)	8	Desert
7	Closed shrubland	47	Shrub
8	Open shrubland (equatorial; arid; warm temperate)	47	Shrub
9	Open shrubland (snow; polar)	42	Shrub/grass (cold)
10	Grassland (snow; polar)	40	Shrub/grass (cool)
11	Savannah (snow; polar)	40	Shrub/grass (cool)
12	Savannah (equatorial; arid; warm temperate)	-	-
13	Grassland (equatorial; arid; warm temperate)	41	Shrub/grass (hot and mild)
14	Woody savannah	32	Dry tropical woods
15	Mixed forest	24	Mixed forest
16	Evergreen broadleaf forest (warm temperate; snow; polar)	25	Cool broadleaf forest
17	Deciduous broadleaf forest (warm temperate; snow; polar)	25	Cool broadleaf forest
18	Deciduous needleleaf forest	21	Conifer boreal forest
19	Evergreen needleleaf forest	22	Conifer
20	Deciduous broadleaf forest (equatorial; arid)	29	Tropical broadleaf
21	Evergreen broadleaf forest (equatorial; arid)	29	Tropical broadleaf
22	Cropland	31	Agricultural
23	Urban and build-up lands	1	Urban
24	Cropland/natural vegetation mosaic	57	Mixed wood/open

* 74 Olson land types are further corresponding to 11 surface types for calculating dry deposition in GEOS-Chem model (Wesely, 1989; Olson, 1992; Jacob et al., 1990, 1992; Wang et al., 1998)

Table S4. Simulated changes in biogenic hydrocarbon emission and soil NO_x emission due to LCLU change, climate change, and combined climate and LCLU change in East Asia. The domain of East Asia is 5.5 °-56.0 °N, 69.0 °-149.0 °E.

Species	CTRL	SIM_LCLU (changes, %)	SIM_CLIM (changes, %)	SIM_COMB (changes, %)
Biogenic hydrocarbons (Tg C yr^{-1})				
Isoprene	34.700	35.635(-2.6)	32.316 (+7.4)	33.271 (+4.3)
Monoterpenes	9.389	9.370 (+0.2)	8.859 (+6.0)	8.855 (+6.0)
Methyl Butenol	0.239	0.241 (-0.7)	0.216 (+11.0)*	0.218 (+9.8) *
Farnesene	0.240	0.252 (-4.8)	0.225 (+6.9)	0.239 (+0.7)
b-Caryophyllene	0.326	0.339 (-3.8)	0.304 (+7.5)	0.320 (+2.2)
Other sesquiterpenes	0.659	0.687 (-4.0)	0.614 (+7.4)	0.650 (+1.9)
Other monoterpenes	1.509	1.482 (+1.8)	1.413 (+6.8)	1.393 (+8.3)
Acetone	5.116	5.173 (-1.1)	4.920 (+4.0)	4.979 (+2.7)
PRPE (lumped >= C3 alkenes)	0.992	1.019 (-2.6)	0.924 (+7.4)	0.952 (+4.3)
Total	53.172	54.199 (-1.9)	49.790 (+6.8)	50.873 (+4.5)
NO_x (Tg N yr^{-1})				
Soil NO_x	2.067	2.053 (+0.7)	2.019 (+2.4)	2.000 (+3.3)
Fertilizer NO_x	0.742	0.741 (+0.1)	0.771 (-3.9)	0.771 (-3.9)
Ozone burden (Tg) (up to 2 km)				
Annual mean in EA	5.638	5.642(-0.071)	5.609(+0.52)	5.615(+0.41)
Summer mean in EA	5.946	5.961(-0.25)	5.795(+2.61)	5.809(+2.36)

References

Anenberg, S. C., Horowitz, L. W., Tong, D. Q., and West, J. J.: An estimate of the global burden of anthropogenic ozone and fine particulate matter on premature human mortality using atmospheric modeling, Environ. Health Persp., 118, 1189-1195, doi:10.1289/ehp.0901220, 2010.

Bartholome, E., Belward, A., Achard, F., Bartalev, S., Carmonamoreno, C., Eva, H., Fritz, S., Gregoire, J.-M., Mayaux, P., and Stibig, H.-J.: GLC 2000: Global Land Cover mapping for the year 2000. Project status November 2002, Institute for Environment and Sustainability, Joint Research Centre, Ispra, Italy, p58, 2002.

Guenther, A. B., Jiang, X., Heald, C. L., Sakulyanontvittaya, T., Duhl, T., Emmons, L. K., and Wang, X.: The Model of Emissions of Gases and Aerosols from Nature version 2.1 (MEGAN2.1): an extended and updated framework for modeling biogenic emissions, Geosci. Model Dev., 5, 1471-1492, doi:10.5194/gmd-5-1471-2012, 2012.

Hurtt, G. C., Chini, L. P., Frolking, S., Betts, R. A., Feddema, J., Fischer, G., Fisk, J. P., Hibbard, K., Houghton, R. A., Janetos, A., Jones, C. D., Kindermann, G., Kinoshita, T., Klein Goldewijk, K., Riahi, K., Shevliakova, E., Smith, S., Stehfest, E., Thomson, A., Thornton, P., Vuuren, D. P., and Wang, Y. P.: Harmonization of land-use scenarios for the period 1500–2100: 600 years of global gridded annual land-use transitions, wood harvest, and resulting secondary lands, Climatic Change, 109, 117-161, doi:10.1007/s10584-011-0153-2, 2011.

Jacob, D. J., and Wofsy, S. C.: Budgets of reactive nitrogen, hydrocarbons, and ozone over the Amazon forest during the wet season, Journal of Geophysical Research: Atmospheres, 95, 16737-16754, doi:10.1029/JD095iD10p16737, 1990.

Jacob, D. J., Wofsy, S. C., Bakwin, P. S., Fan, S. M., Harriss, R. C., Talbot, R. W., Bradshaw, J. D., Sandholm, S. T., Singh, H. B., Browell, E. V., Gregory, G. L., Sachse, G. W., Shipham, M. C., Blake, D. R., and Fitzjarrald, D. R.: Summertime photochemistry of the troposphere at high northern latitudes, J. Geophys. Res.-Atmos., 97, 16421-16431, doi:10.1029/91JD01968, 1992.

Jerrett, M., Burnett, R. T., Pope, C. A., Ito, K., Thurston, G., Krewski, D., Shi, Y., Calle, E., and Thun, M.: Long-Term Ozone Exposure and Mortality, New Engl. J. Med., 360, 1085-1095, doi:10.1056/NEJMoa0803894, 2009.

Loveland, T. R., Reed, B. C., Brown, J. F., Ohlen, D. O., Zhu, Z., Yang, L., and Merchant, J. W.: Development of a global land cover characteristics database and IGBP DISCover from 1 km AVHRR data, Int. J. Remote Sens., 21, 1303-1330, doi:10.1080/014311600210191, 2000.

Liu, J. Y., and Buheaosier: Study on spatial-temporal feature of modern land -use change in China: Using Remote Sensing techniques, Quaternary Sciences, 20 (3), 229-239, 2000.

Liu, J. Y., Liu, M., Tian, H., Zhuang, D., Zhang, Z., Zhang, W., Tang, X., and Deng, X.: Spatial and temporal patterns of China's cropland during 1990–2000: An analysis based on Landsat TM data, Remote Sensing of Environment, 98, 442-456, doi:10.1016/j.rse.2005.08.012, 2005a.

Liu, J. Y., Tian, H. Q., Liu, M. L., Zhuang, D. F., Melillo, J. M., and Zhang, Z. X.: China's changing landscape during the 1990s: Large-scale land transformations estimated with satellite data, Geophys. Res. Lett., 32, L02405, doi: 10.1029/2004gl021649, 2005b.

Liu, M. L., and Tian, H. Q.: China's land cover and land use change from 1700 to 2005: Estimations from high-resolution satellite data and historical archives, Global Biogeochem. Cy., 24, GB3003, doi:10.1029/2009gb003687, 2010.

Olson, J.: World Ecosystems (WE1.4). Digital Raster Data on a 10-minute Geographic 1080x2160 grid, in: Global Ecosystems Database, Version 1.0: Disc A., edited by: NOAA National Geophysical Data Center, Boulder, Colorado., 1992.

Silva, R. A., West, J. J., Zhang, Y., Anenberg, S. C., Lamarque, J.-F., Shindell, D. T., Collins, W. J., Dalsoren, S., Faluvegi, G., Folberth, G., Horowitz, L. W., Nagashima, T., Naik, V., Rumbold, S., Skeie, R., Sudo, K., Takemura, T., Bergmann, D., Cameron-Smith, P., Cionni, I., Doherty, R. M., Eyring, V., Josse, B., MacKenzie, I. A., Plummer, D., Righi, M., Stevenson, D. S., Strode, S., Szopa, S., and Zeng, G.: Global premature mortality due to anthropogenic outdoor air pollution and the contribution of past climate change, Environ. Res. Lett., 8, 034005, 2013.

Stavrakou, T., Müller, J. F., Bauwens, M., De Smedt, I., Van Roozendael, M., Guenther, A., Wild, M., and Xia, X.: Isoprene emissions over Asia 1979-2012: impact of climate and land-use changes, Atmos. Chem. Phys., 14, 4587-4605, doi:10.5194/acp-14-4587-2014, 2014.

Steinkamp, J., and Lawrence, M. G.: Improvement and evaluation of simulated global biogenic soil NO emissions in an AC-GCM, Atmos. Chem. Phys., 11, 6063-6082, doi:10.5194/acp-11-6063-2011, 2011.

Wang, Y., Jacob, D. J., and Logan, J. A.: Global simulation of tropospheric O_3-NO_x-hydrocarbon chemistry 1 Model formulation, J. Geophys. Res., 103, 10713-10725, 1998.

Wesely, M. L.: Parameterization of surface resistances to gaseous dry deposition in regional-scale numerical models, Atmos. Environ., 23, 1293-1304, doi:10.1016/0004-6981(89)90153-4, 1989.